Proceedings of ICFDP9:
Ninth International Congress of Fluid Dynamics & Propulsion
December 18-21, 2008, Alexandria, Egypt

ICFDP9-EG-274

AERODYNAMIC INVESTIGATION OF A CONCAVED AIRFOIL IN GROUND EFFECT

K. A. Hafez
Department of Naval Architecture and Marine Engineering, Faculty of Engineering, Alexandria University, P.C. 21544 El-Shatbi, Alexandria, Egypt

O. A. Elsamni
Department of Mechanical Power Engineering, Faculty of Engineering, Alexandria University, P.C. 21544 El-Shatbi, Alexandria, Egypt

P. A. Hung and H. H. Chun
Advanced Ship Engineering Research Center, Pusan National University, San 30, Jangjeon-Dong, Gumjeong-Gu, Busan, 609-735, Korea

ABSTRACT

The present paper investigates the aerodynamic characteristics of an arbitrary airfoil and its impact on the performance of a Ground Effect Vehicle *GEV*. The approaches that have been previously suggested and conducted for studying the *WIG* problem are demonstrated. Few published papers are accompanied by reasonable background information to enable an independent researcher to directly incorporate the available mathematical model into his calculations. A numerical technique for investigating the aerodynamic characteristics of an arbitrary airfoil in the ground effect zone is adapted. Wide ranges of the dominant parameters, i.e., ground clearance, angle of attack and *Reynolds* number are considered. The calculations are performed within the framework of a *2-D* formulation to provide a simple mathematical model with a meaningful physical interpretation of the numerical results. Prominence is given to the investigation of the numerical results and there physical interpretation rather than to the method of calculating a particular result. Validation of the present numerical results against the available published researches is clarified. Finally, for the whole effort to be demonstrated efficiently the results obtained are analyzed, the conclusions are presented, and few important future amendments are suggested. Parenthetically, the authors are venture to suggest that this research represents a keystone to a more rational and practical prediction of the aerodynamic characteristics of an arbitrary airfoil.

KEYWORDS:

Wing in Ground Effect *WIG*; Ground Effect Vehicle *GEV*; Wing in Surface Effect *WISE*; Computational Fluid Dynamics *CFD*, Vortex; Drag; Lift.

INTRODUCTION

The aerodynamic characteristics of a wing in ground effect *WIG* are of special interests because of their wide applications not only for the airplanes during their landing and take-off, but also for the high speed marine wing in surface effect vehicles *WISE*. The *WISE* vehicle has two main advantages, its ability to carry a massive payload as a marine vehicle, but to cruise at the speed of an aircraft; and its ability to fly at very low altitudes, below the detection range of the inconvenient radars. When the wing with small angles of attack operates in the proximity of the ground, favorable aerodynamic characteristics are revealed. The lift increases due to the generation of a high-pressure air cushion "ram effect" or "ram pressure" under the wing, whereas the drag decreases due to the reduction of the induced downwash velocity. Consequently, the *GEV* efficiency increases, with the result that the flight range of a *WIG* vehicle is longer than that of a conventional aircraft for the same fuel consumption. In other words, the higher the lift-to-drag ratio, the higher the efficiency of the *WIG* vehicle and the lower its fuel consumption for a given weight. However, in reality for a *WISE* vehicle working at lower altitudes above the sea surface where the air is denser, it may take more time to reach its destination comparable to an aircraft operating at high altitude.

Several theoretical and numerical studies including *2-D* and *3-D* steady and unsteady calculations were performed to identify the aerodynamic characteristics of the *WIG* [1-7]. However, the focus of the earlier studies directed to the inviscid flow by using either the panel method or the lifting surface model. Aside from the inviscid flow approach, Hsiun and Chen [3, 4] considered the numerical analysis of the steady *2-D WIG* effect in the laminar viscous flow. They concluded that the

airfoil with larger camber and smaller thickness induces a higher lift-to-drag ratio. Recently, Moon et el. [7] investigated numerically the *3-D* cambered wing of *NACA 4406* with an angle of attack *2°*. *Reynolds* number based on the chord length was set at 2×10^6. They focused on the dependency of the flow structure on the configuration of the main and vertical wings by which the high lift-to-drag ratio changes.

Several experimental studies were conducted aiming at examining the dependency of forces acting on different wing configurations with different ground clearances [8-16]. Of interest is the recent experiment of Ahmed and Sharma [16] who examined the flow around the symmetrical airfoil *NACA 0015*. Various angles of attack ranges as $0^o \le \alpha \le 10^o$ were considered while the clearance varies from the minimum possible value to around one chord length. They showed that high values of pressure coefficients appear on the lower surface by decreasing the ground clearance, leading to high lift when the wing is close to the ground. Their results suggested that the pressure distribution on the upper surface does not change significantly at higher incident angles regardless of the ground clearance variation.

Further investigations on the development and the stability analysis of a *GEV* were done [17-20]. Although numerous computational researches had investigated the *WIG* problem, only few researches considered the flow in the vicinity of the airfoil, at high *Reynolds* number. Palpably, the survey of the literature suggests that the *WIG* problem needs to be carried out for high *Reynolds* numbers.

Therefore the present study investigates numerically the aerodynamic characteristics of the *2-D* wings in the vicinity of the ground by solving the *2-D* incompressible *Navier–Stokes* equations with the appropriate turbulence model. The aerodynamic characteristics of various *2-D NACA four-digit* profiles are examined by considering their camber and thickness effects to select the most efficient airfoil profile that gives maximum performance in ground effect. The effect of the ground clearance ranges as $0.1 \le h/C \le 1.25$ for various angles of attack ranges as $0^o \le \alpha \le 30^o$ on the aerodynamic characteristics of the selected airfoil profile is investigated. Finally, for the specified conditions of the ground clearance and the angle of attack where the highest efficiency of the *GEV* vehicle is obtained, the effect of the *Reynolds* number on the aerodynamic characteristics is investigated.

COMPUTATIONAL DETAILS

The governing equations describing the steady incompressible and viscous flow field are the continuity and *Reynolds* averaged *Navier-Stokes* equations (1) and (2)

$$\frac{\partial U_i}{\partial x_i} = 0.0 \tag{1}$$

$$\frac{\partial}{\partial x_j}\left(\rho U_i U_j\right) = -\frac{\partial P}{\partial x_i} + \frac{\partial}{\partial x_j}\left[\mu\left(\frac{\partial U_i}{\partial x_j} + \frac{\partial U_j}{\partial x_i}\right)\right] + \frac{\partial}{\partial x_j}\left(-\rho\overline{u_i' u_j'}\right) \tag{2}$$

The relatively recent *realizable* $k-\varepsilon$ model proposed by Shih et al. [21] is adopted because it contains a new formulation for the turbulent viscosity as proposed by Reynolds [22], and a new transport equation for the dissipation rate, ε, based on an exact dynamic equation for the transport of the mean square vorticity fluctuation. The term realizable means that the model satisfies certain mathematical constraints on the *Reynolds* stresses, consistent with the physics of turbulent flows.

Initial studies have shown that the realizable model provides the best performance for several validations of separated flows and flows with complex secondary flow features. An immediate benefit of the realizable $k-\varepsilon$ model is that it more accurately predicts the spreading rate of both planar and round jets. Also it provides superior performance for flows involving rotation, vortices, and strong streamline curvature, boundary layers under strong adverse pressure gradients, separation, and recirculation. It is believed that the present form better represents the spectral energy transfer.

The realizable $k-\varepsilon$ model has been extensively validated for a wide range of flows [21,23], including rotating homogeneous shear flows, free flows including axisymmetric and planar jets, mixing layers, channel and boundary layer flows, and separated flows. The *Reynolds* averaged *Navier-Stokes* equations and the transport equations for the turbulent kinetic energy and dissipation rate are solved by the *SIMPLE* algorithm with a second-order spatial discretization scheme that based on finite volume method. No–slip boundary conditions are imposed on the surface of the wing, whereas the symmetry condition is set for the far-field boundary. The uniform flow with a free-stream velocity U_∞ and low turbulent intensity are applied on the inflow boundary while the convective boundary condition is applied at the outflow boundary. The ground surface is considered as a moving wall boundary at the free-stream velocity.

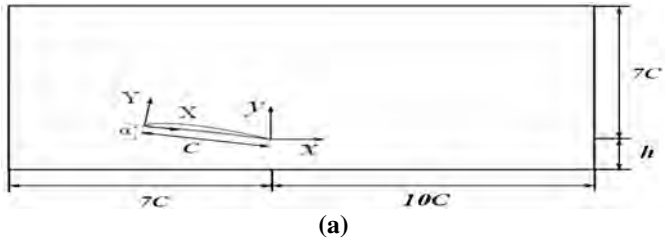

(a)

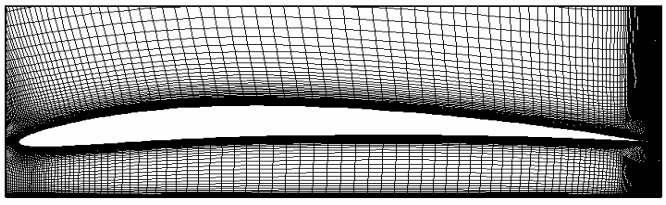

(b)

Fig. 1. (a) Physical model of the *2-D WIG* problem, the computational domain and coordinate system, and (b) Grid system near the wing and ground for $\alpha = 0^\circ$ and $h/C = 0.1$

Table 1. Grid-dependency for *2-D NACA 4406* airfoil at $\alpha = 2^{\circ}$ and $h/C = 0.1$

	C_L	C_D	$f = C_L/C_D$
Grid-A	0.8408	0.00993	84.6727
Grid-B	0.8411	0.00977	86.0901
Grid-C	0.8414	0.00976	86.2090

The size of the computational domain is defined as $-7C \le x \le 10C$ and $-h \le y \le 7C$ for the streamwise and vertical directions, respectively, where C is the chord length of the wing. In case of the isolated wing, the domain size is increased to $-7C \le y \le 7C$ in the vertical direction. Fig. 1(a) shows the physical model of the *2-D WIG* problem, the size of the computational domain, and the coordinate system.

The minimum vertical grid spacing on both the wing and the ground surface is chosen to be about $10^{-4}C$ at the same *Reynolds* number of 2×10^{6}, similar to that of Moon *et al.* [7]. In order to capture accurately the separating shear layers on both the wing and the ground, the grids are distributed non-uniformly near these regions, especially in the gap and the wake regions. To consider the variation of ground clearance, dense resolutions are maintained near both the wing and the ground surface and also in the area under the wing. Fig. 1(b) shows the grid distribution near the wing corresponding to an angle of attack $\alpha = 0^{\circ}$ at a ground clearance of $h/C = 0.1$, and the ground surface. The number of the grid points used in the y direction is tuned up to maintain a dense resolution near the wing, moving wall and also in the gap spacing, which in turn reflects the variation of the gap ratio. The commercial *CFD* package namely *FLUENT 6.2* is employed for all numerical calculations.

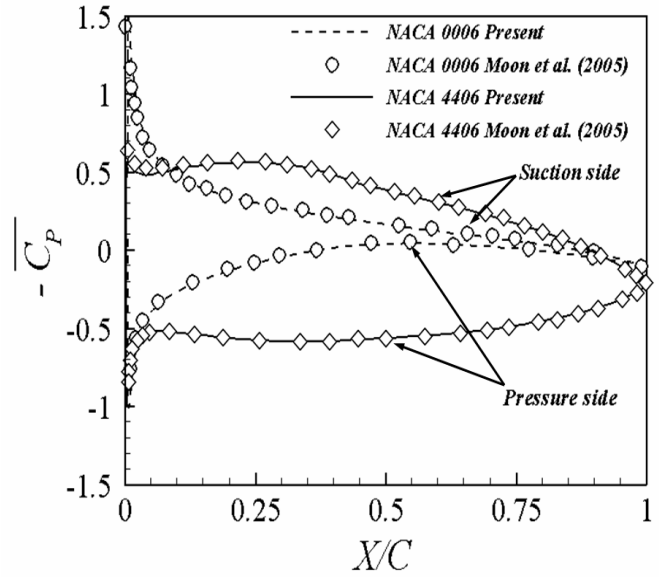

Fig. 2. Distributions of mean pressure coefficient on the surface of *2-D NACA 0006* and *NACA* 4406 airfoils for $\alpha = 2^{\circ}$ and $h/C = 0.1$

Table 2. Aerodynamic characteristics of *2-D NACA four digits* airfoils in ground effect

	C_L	C_D	$f = C_L/C_D$
NACA 4406	0.8411	0.0099	84.9596
NACA 4409	0.7964	0.0107	74.4299
NACA 4412	0.7223	0.0119	60.6975
NACA 4415	0.6050	0.0136	44.4853
NACA 4418	0.4293	0.0162	26.5000

The grid-dependency is tested with the coarse, medium and finer grids of 1.5×10^{4} *(grid-A)*, 3×10^{4} *(grid-B)* and 4.5×10^{4} *(grid-C)*, respectively. Table 1 shows the lift and drag coefficients, and the *GEV* efficiency for the different grid sets. The comparison indicates that *grid-B* and *grid-C* provide almost similar results on the price of more calculation time. Therefore, *grid-B* is seen to be reasonable for flow predictions and it will be used for the present calculations.

Validation of the present computational method is performed for two different *2-D* wings *NACA 0006* and *NACA 4406* at $\alpha = 2^{\circ}$ and $h/C = 0.1$. In this regard, Fig. 2 shows that the distribution of the mean pressure coefficient C_P over the wing surfaces agrees well with that of Moon *et al.* [7]. This in turn indicates the adequacy of the present calculation method for the analysis of the turbulent flow in *WIG* problem.

SELECTION OF THE AIRFOIL PROFILE

The present study started by testing numerically five different *2-D* wings *NACA 4406*, *NACA 4412*, *NACA 4412*, *NACA 4415* and *NACA 4418* that shown in Fig. 3. The

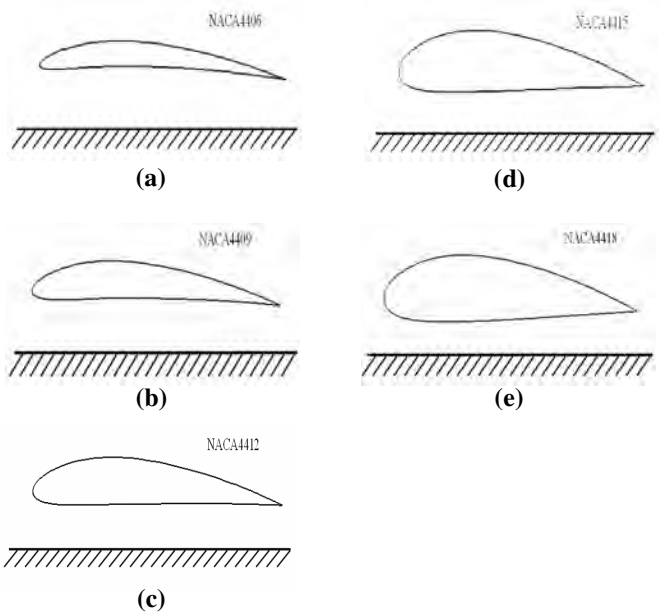

Fig. 3. Profiles of five different *2-D NACA four digits* airfoils in ground effect. (a) *NACA 4406*, (b) *NACA 4409*, (c) *NACA 4412*, (d) *NACA 4415*, and (e) *NACA 4418*

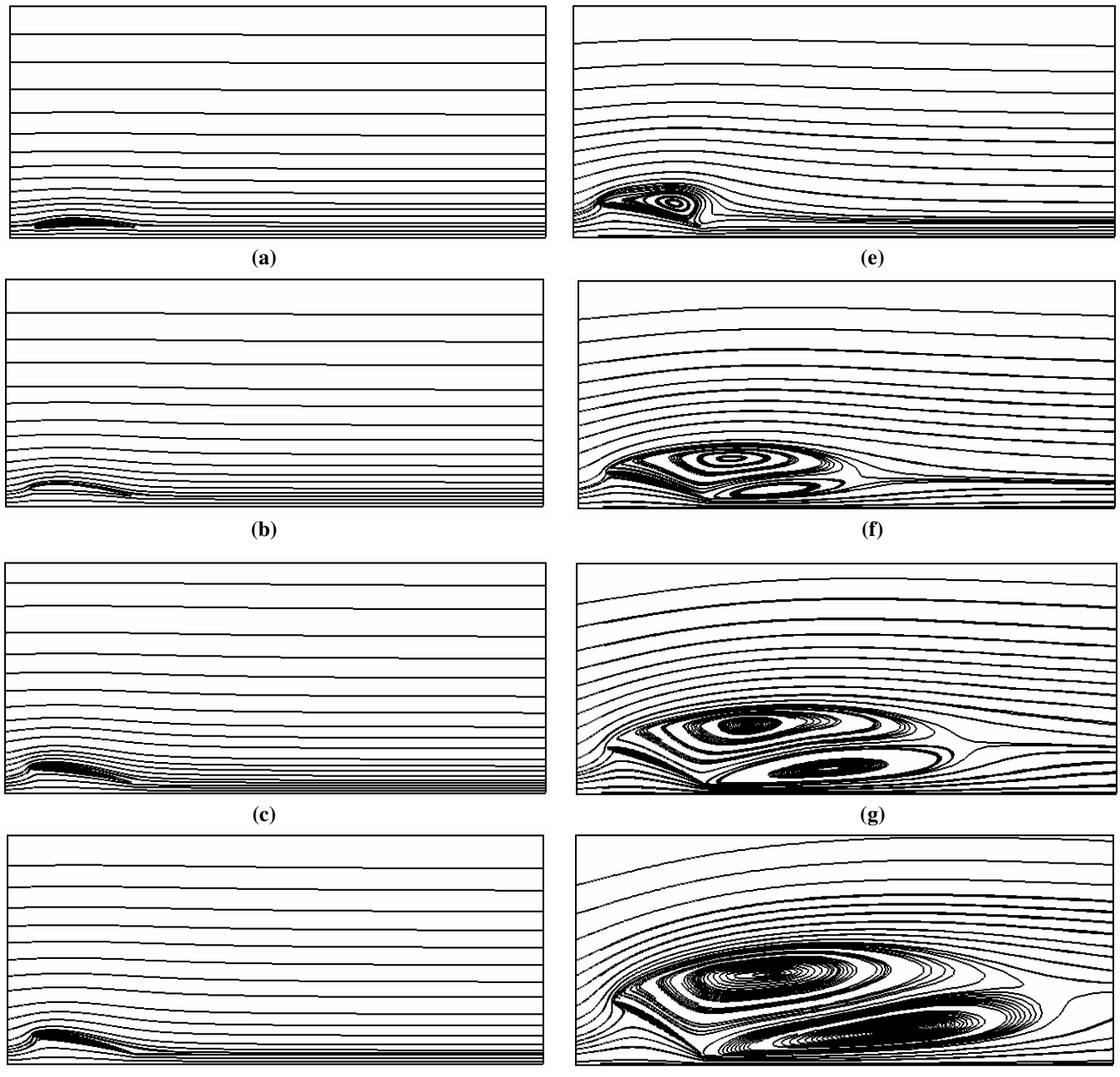

Fig. 4. Mean streamlines around the *NACA 4406* airfoil at $h/C = 0.1$ for **(a)** $\alpha = 0^{\circ}$, **(b)** $\alpha = 4^{\circ}$, **(c)** $\alpha = 8^{\circ}$, **(d)** $\alpha = 10^{\circ}$, **(e)** $\alpha = 12^{\circ}$, **(f)** $\alpha = 14^{\circ}$, **(g)** $\alpha = 20^{\circ}$ and **(h)** $\alpha = 30^{\circ}$

maximum camber deflection of the tested wings is 4.0% of the chord, and located at 40% of their chord. This preliminary test is performed at $\alpha = 2^{\circ}$, $h/C = 0.1$ and $R_e = 2 \times 10^6$ with the incoming turbulent intensity of 0.10% and aims at selecting a profile with the highest value of the *GEV* efficiency.

Table 2 shows the lift and drag coefficients, and the lift-to-drag ratio for the aforementioned five airfoil profiles. The lift is found to be higher for the profiles with smaller thicknesses. The maximum lift coefficient of about 0.84 is found to be for *NACA 4406*, whereas for the largest thickness profile of *NACA 4418* a lift coefficient of nearly 0.43 is obtained. The drag coefficient increases as the thickness of the airfoil increases. The trend of the lift and drag coefficients for the different aforementioned five profiles is similar to that shown in previous

studies [13, 16]. Also, comparing their aerodynamic performance indicates that the *NACA 4406* gives the best performance with lift-to-drag ratio of about 86.

RESULTS AND DISCUSSION

Selecting *NACA 4406* for the present *2-D WIG* problem, six different ground clearances range as $0.1 \le h/C \le 1.25$ and twelve different angles of attack range as $0^o \le \alpha \le 30^o$ are investigated. The flow corresponds to *Reynolds* number $R_e = 2 \times 10^6$ and has the incoming turbulent intensity of 0.1%.

PATTERNS OF THE FLOW

The mean streamlines around the wing at the smallest ground clearance $h/C = 0.1$ for different angles of attack are shown in Figs. 4(a-h). In the range of $0° \le \alpha \le 10°$, the streamlines do not show separation along the wing surface. The stagnation point gradually moves from the leading edge to the lower surface with increasing the angle of attack as shown in Figs. 4(a-d).

As α exceeds $10°$, the mean flow patterns change significantly due to the appearance of the vortices over the upper surface of the wing. For $\alpha = 12°$, a clockwise rotating vortex is formed over the upper surface after the flow separation at the leading edge as shown in Fig. 4(e).

As α increases to $14°$, the flow separation is more significant which results in increasing the size and the strength of the primary vortex rotating in the clockwise direction. Moreover, a secondary vortex appears between the primary vortex and the moving wall as shown in Fig. 4(f). It seems that a jet-like flow is initiated in the gap between the trailing edge and the moving wall which is strong enough to separate the flow at the trailing edge for this angle of attack.

Further increasing α, the size of the primary and secondary vortices become considerably larger and successively elongate downstream with the formation of stronger shear layers as can be clarified by comparing with the cases of

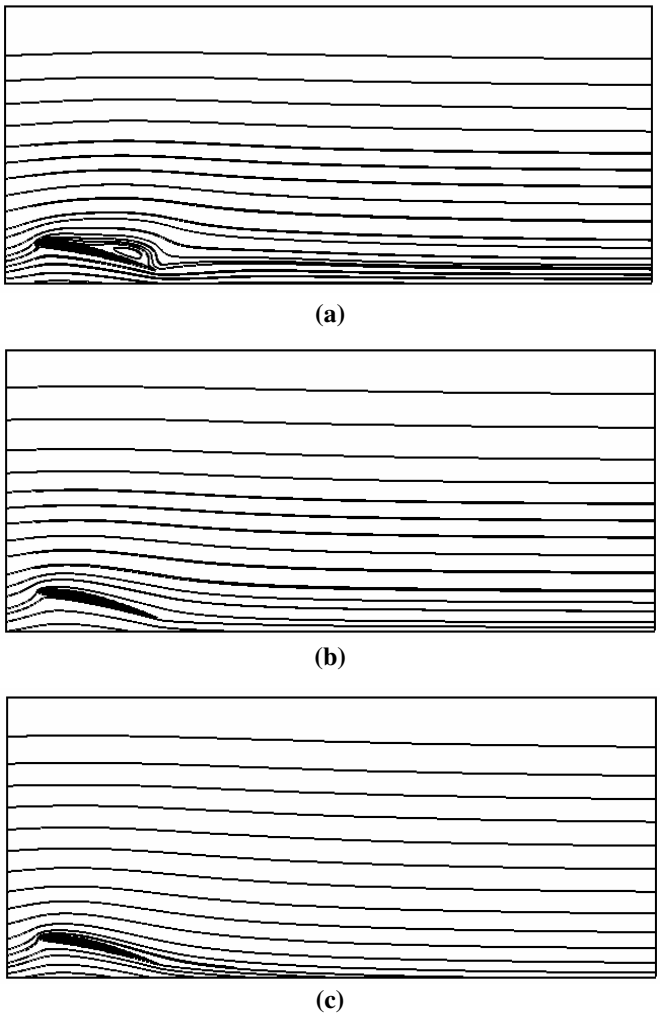

(a)

(b)

(c)

Fig. 5. Mean streamlines around the *NACA 4406* airfoil for $\alpha = 12^\circ$ at (a) $h/C = 0.25$, (b) $h/C = 0.5$, and (c) $h/C = 1.25$

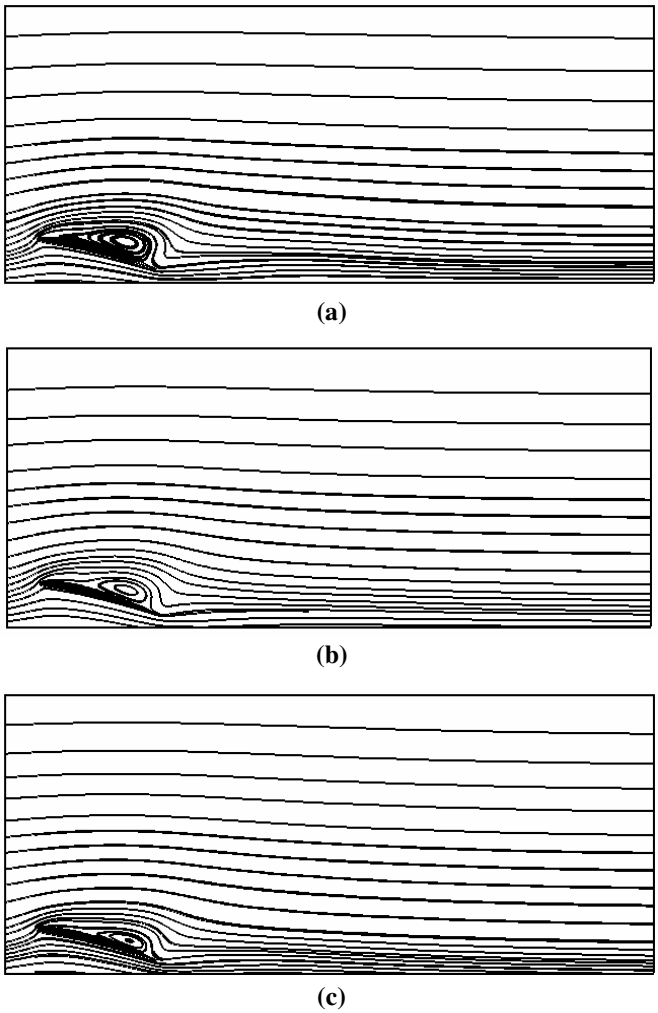

(a)

(b)

(c)

Fig. 6. Mean streamlines around the *NACA 4406* airfoil for $\alpha = 14^\circ$ at (a) $h/C = 0.25$, (b) $h/C = 0.5$ and (c) $h/C = 1.25$

$\alpha = 14°, 20°, and 30°$ plotted in Figs. 4(f-h).

In the range of $0° \le \alpha \le 10°$, the dependency of the mean flow on h/C is very weak and the mean flow patterns for different h/C's are much similar to those shown in Figs. 4(a-d) and hence they are omitted here for brevity. However, when α is larger than $10°$, the mean flow patterns are strongly modified by increasing h/C.

Thus, representatively the cases of $\alpha = 12°, and 14°$ are considered to observe the effect of h/C on the mean flow since the dependence of the mean flow on h/C for other high α's is much similar to the case of $\alpha = 14°$.

Fig. 5 shows the mean streamlines around the wing for $\alpha = 12°$ and $h/C = 0.25, 0.50, and 1.25$. The vortex appearing over the upper surface of the wing at $h/C = 0.10$, as already shown in Fig. 4(e), diminishes with increasing h/C up to 0.5 as observed by moving from Fig. 5(a) to Fig. 5(b). Since the increase of the ground clearance results in diminishing the jet-like flow that in turn predominates the downwash flow from the upper surface and consequently leads to the suppression of the vortex over the upper surface of the wing. With further increasing h/C, the vortex is expected to disappear completely, as may be noticed for example at $h/C = 0.5$ in Fig. 5(b). Moreover, the formation of the mean streamlines at $h/C > 0.5$ doesn't change significantly from that at $h/C = 0.5$ as shown in Fig. 5(c).

Fig. 6 shows the mean streamlines around the wing at $\alpha = 14°$ and for $0.25 \le h/C \le 1.25$. The primary vortex appears over the upper surface of the wing at $h/C = 0.10$, already shown in Fig. 4(f), diminishes with increasing h/C up to 0.25 as observed in Fig. 6(a). Palpably, the secondary vortex observed at the smallest $h/C = 0.10$ doesn't exist at $h/C = 0.25$. With further increasing h/C up to 1.25, the primary vortex becomes smaller and moves toward the trailing edge of the airfoil as shown in Figs. 6(b, c). Similar variations of the flow patterns including the vortices initiation and propagation for different h/C are also observed at higher values of $\alpha = 20°, and 30°$, but excluded from this research for the brevity purposes.

PRESSURE DISTRIBUTION OVER THE WING SURFACE

Fig. 7 shows the variation of the mean pressure coefficient $\overline{C_P}$ along the wing surface for different h/C's at four different angles of attack $\alpha = 0°, 4°, 8°, and 10°$. In the case of $\alpha = 0°$, near the leading edge, i.e., for $x/C < 0.05$, suction and pressure behaviors take place on the lower and the upper surfaces of the airfoil, respectively, regardless the values of h/C. The suction peek at the airfoil nose indicates that separation is likely to occur there, which confirms with the fact that the nose radius of the airfoil must not be too small as this may lead to very early separation in a probable strong ground effect. The value of $-\overline{C_P}$ on the lower surface is higher than that on the upper surface as shown in Fig. 7(a). After passing the region near the leading edge, i.e., for $x/C > 0.05$, the pressure on the lower surface becomes higher than that on the upper surface. Since the cambered wing has a high flow divergence, the higher pressure is distributed on the lower surface along the chord length except the region close to the leading edge for $x/C < 0.05$.

As an angle of attack is allowed for, the distribution of $\overline{C_P}$ is considerably changed from that for $\alpha = 0°$, especially near the leading edge, as shown in Figs. 7(b-d). However, in the range of $0° < \alpha \le 10°$, it can be assured from Figs. 7(b-d) that a similar pattern of $\overline{C_P}$ variation along the wing surface corresponding to h/C occurs, which may be supported by a similar flow pattern as already observed in Figs.4 (b-d).

In the proximity of the leading edge on the upper surface of the wing, the pressure becomes very low because the suction effect becomes strong due to the movement of the stagnation point toward the lower surface with increasing α. Figs. 7(b-d) show that the high positive value of $-\overline{C_P}$ appears in the proximity of the leading edge. As we move toward the trailing edge on the upper surface of the wing, the pressure augments. As h/C increases at fixed α, the pressure on the upper surface slightly decreases at a reduction rate increases as α increases.

In the proximity of the leading edge on the lower surface of the wing, the pressure changes rapidly from the low state to the high state, correspondingly the positive value of $-\overline{C_P}$ decreases quickly as the negative one. After the pressure reaches its maximum value in the proximity of the leading edge on the lower surface, it slightly decreases. As α increases, the location of the maximum pressure corresponding to the negative peak of $-\overline{C_P}$ becomes more distant due to the movement of the stagnation point toward the lower surface, which can be clarified by the comparing Figs. 7(b-d). At a specific α, increasing h/C especially in the range of $0.10 \le h/C \le 0.75$, decreases the pressure on the lower surface clearly. However, any further increment in h/C from 0.75 to 1.25 doesn't reflect any considerable variation in the pressure over the lower surface.

Fig. 8 shows the variation of the mean pressure coefficient $\overline{C_P}$ on the wing surface at different h/C's for four different angles of attack $\alpha = 12°, 14°, 20°, and 30°$. When α exceeds $10°$, the pressure distribution depends strongly on the vortex formed over the upper surface of the wing which already observed in Figs. 4(e-h). In the case of $\alpha = 12°$, for low ground clearances of $h/C = 0.1$ and 0.25, the profile of $\overline{C_P}$ on the upper surface depicts two peaks with the low pressure as revealed in Fig. 8(a). One peak locates at $x/C = 0.65$, i.e., near the vortex center where the reverse flow accelerates. When x/C approaches the reattachment location at about $x/C = 0.87$ as previously shown in Fig. 4(e), the pressure increases again, leading to forming the minimum of $-\overline{C_P}$ over the upper surface of the wing as observed in Fig. 8(a). After passing the reattachment location, the flow starts to accelerate, with the result that the other peak of $-\overline{C_P}$ appears near the trailing edge. Consequently, the pressure distribution over the

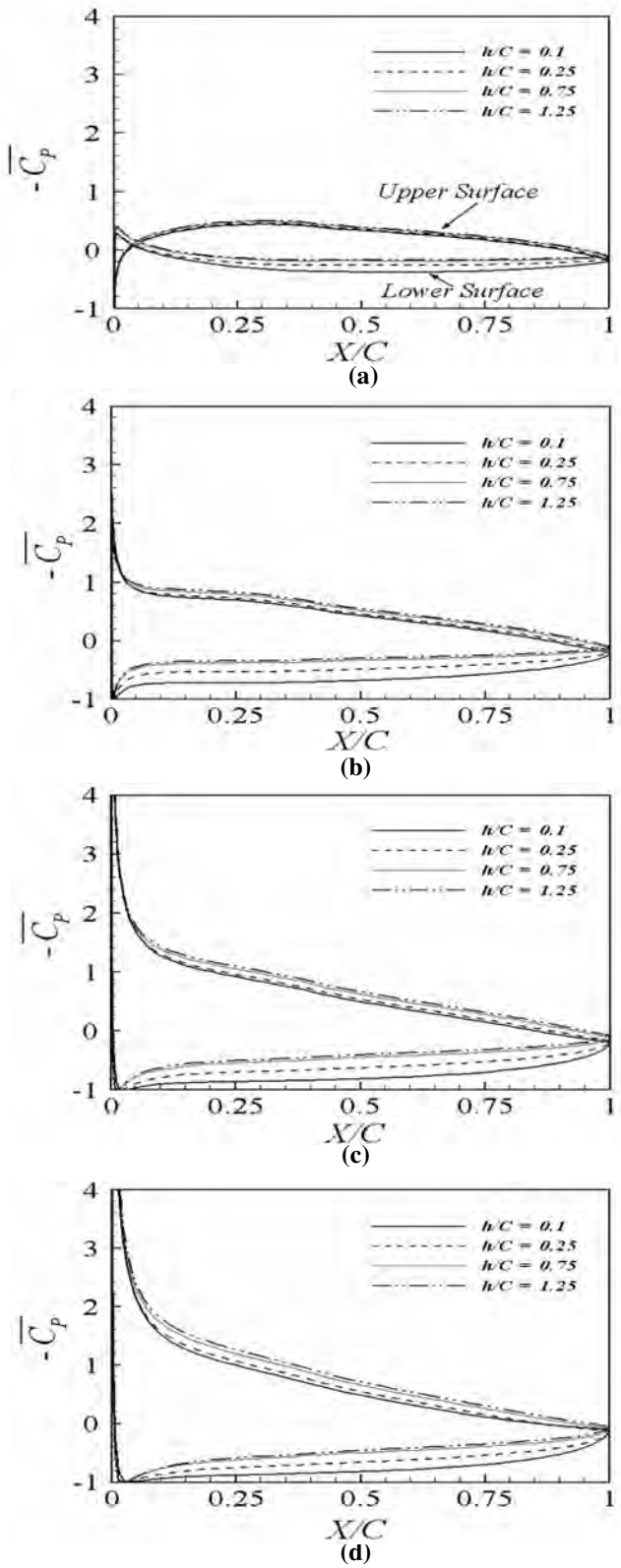

Fig. 7. Distribution of the mean pressure coefficient on the surface of the *NACA 4406* airfoil for different ground clearances at (a) $\alpha = 0°$, (b) $\alpha = 4°$, (c) $\alpha = 8°$, and (d) $\alpha = 10°$

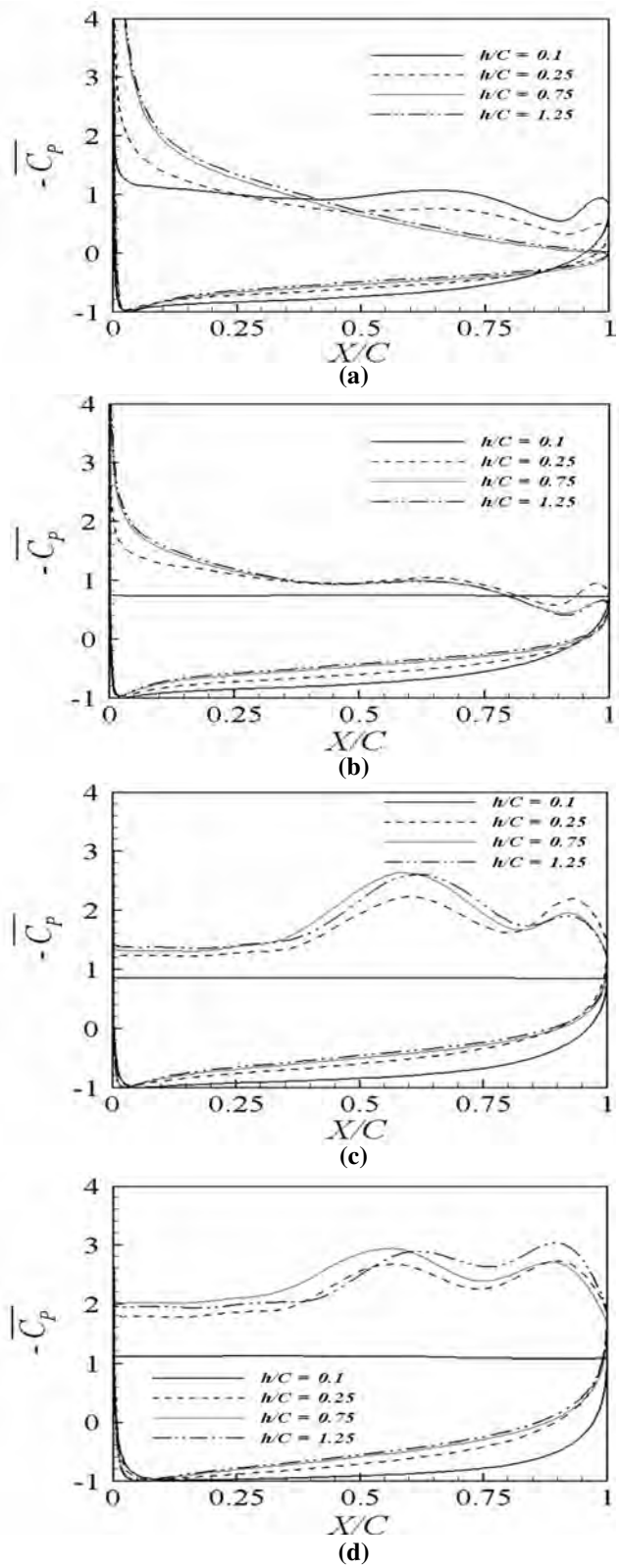

Fig. 8. Distribution of the mean pressure coefficient on the surface of the *NACA 4406* airfoil for different ground clearances at (a) $\alpha = 12°$, (b) $\alpha = 14°$, (c) $\alpha = 20°$, and (d) $\alpha = 30°$

lower surface deceases quickly as x/C approaches the trailing edge. When the vortex disappears on the upper surface, for

example at $h/C = 0.75, and 1.25$, the profile of $\overline{C_P}$ on the wing surface has almost the same pattern as the cases of $0° < \alpha \le 10°$, which can be clarified by comparing Fig. 8(a) and Figs. 7(b-d).

In the case of $\alpha = 14°$, at the low ground clearance of $h/C = 0.1$, since the center of the primary vortex locates far away from the upper surface as already shown in Fig. 4(f), the large reverse flow without the severe local variation of velocity covers the entire upper surface of the wing. Therefore, the pressure distributes uniformly over the upper surface with the low value of the $-\overline{C_P}$ flat profile corresponds to the positive value on the upper surface as shown in Fig. 8(b). As h/C increases, the vortex resolute and its center comes closer to the upper surface as shown in Fig. 6, which is comparable with the cases of the low ground clearances of $h/C = 0.1, and 0.25$ at $\alpha = 12°$. Consequently, the pressure distribution over the wing surface shows clear similarity with the cases of $h/C = 0.1, and 0.25$ at $\alpha = 12°$.

Further increasing α to 20°, and 30°, as already mentioned, the flow pattern - including the vortex evolution - varies with respect to h/C in a manner similar to the case of $\alpha = 14°$. As a result, a similar pattern of $\overline{C_P}$ variation with respect to h/C occurs at $\alpha = 14°, 20°, and 30°$ as shown in Figs. 8(b-d). However, increasing α, especially on the upper surface of the wing, decreases the pressure significantly.

COEFFICIENTS OF FORCES

Fig. 9 shows the lift coefficient C_L as a function of h/C for different angles of attack which expand over two regions defined as $0^o \le \alpha \le 10^o$ and $12^o \le \alpha \le 30^o$. In the range $0^o \le \alpha \le 10^o$, the maximum C_L occurs at the lowest h/C of 0.1 after that C_L decreases with increasing h/C. Finally, C_L tends to be constant as h/C reaches 0.75, whereas at constant h/C, C_L shows augmentation as α increases, and the reduction rate of C_L reduces with increasing α as shown in Fig. 9(a).

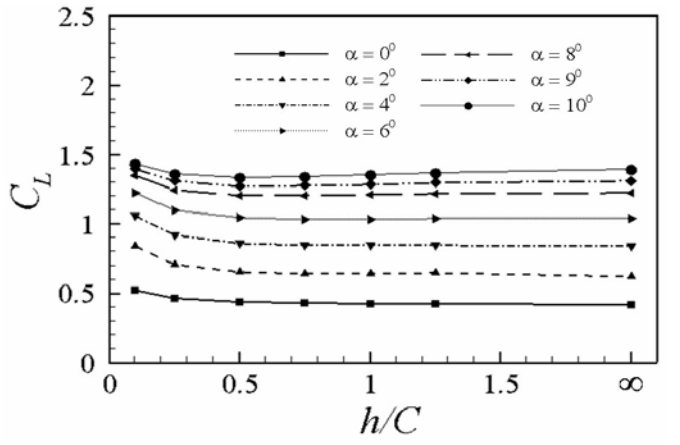

(a)

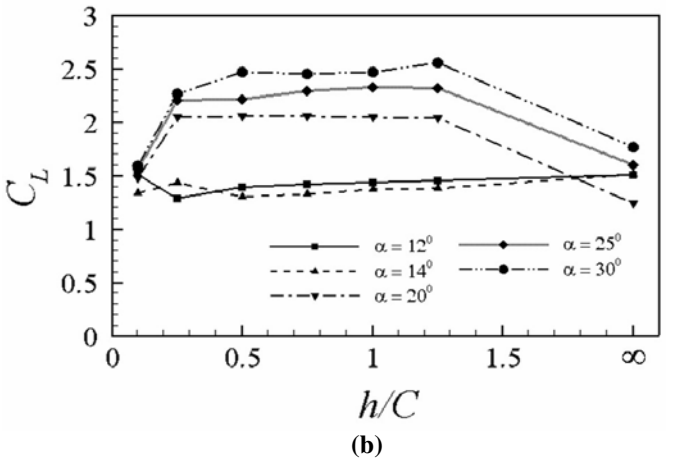

(b)

Fig. 9. Lift coefficient as a function of the ground clearance for different angles of attack in the range of (a) $0^\circ \le \alpha \le 10^\circ$, and (b) $12^\circ \le \alpha \le 30^\circ$

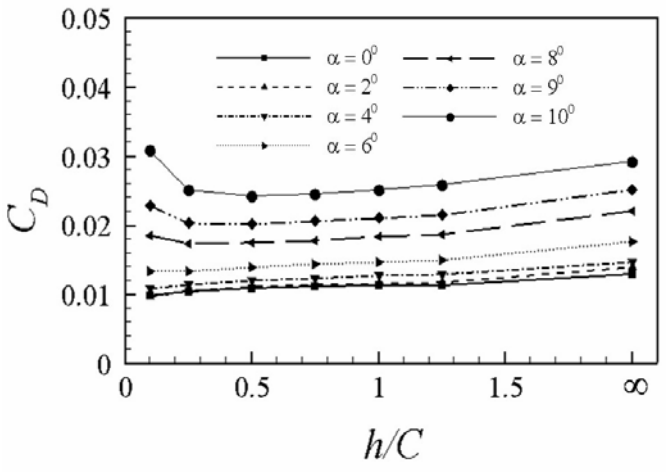

(a)

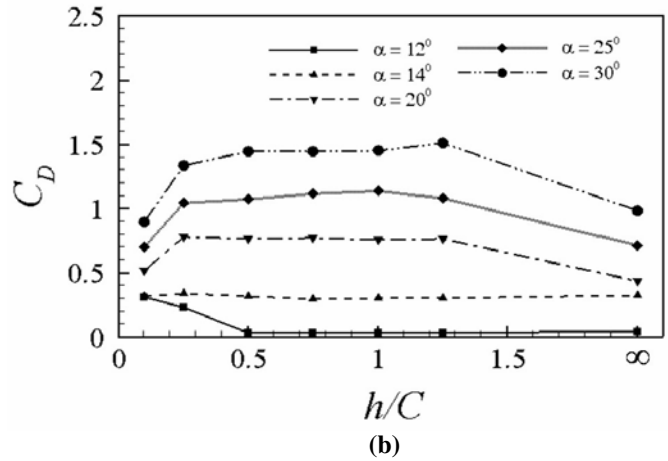

(b)

Fig. 10. Drag coefficient as a function of the ground clearance for different angles of attack in the range of (a) $0^\circ \le \alpha \le 10^\circ$, and (b) $12^\circ \le \alpha \le 30^\circ$

For $\alpha = 12°$, the pattern of the variation of C_L with respect to h/C is the same with the cases of the range $0^o \le \alpha \le 10^o$, which shows that the maximum C_L occurs at the lowest h/C of 0.1. In contrast to the cases of $0^o \le \alpha \le 12^o$, the cases of $\alpha \ge 14^\circ$ reveal the minimum C_L at the lowest h/C of 0.1. As h/C increases, C_L increases significantly and eventually converges as h/C gets higher as shown in Fig. 9(b).

The drag coefficient C_D as a function of h/C for different angles of attack is plotted in Fig. 10. The order of C_D for $0^o \le \alpha \le 10^o$ in Fig. 10(a) is significantly smaller than that of C_D for $12^o \le \alpha \le 30^o$ in Fig. 10(b) since the formed drag increases considerably as α increases.

At a constant α in the range $0^o \le \alpha \le 6^o$, C_D slightly increases with increasing h/C as shown in Fig. 10(a). For $\alpha = 8°,9°,and 10°$, C_D has a maximum at the lowest h/C of 0.1 and then it decreases by moving towards $h/C = 0.25$. For $h/C = 0.25$, the values of C_D are almost the same for the cases of $\alpha = 8°,9°,and 10°$ as shown in Fig. 10(a). At constant h/C, C_D increases slightly as α increases. In contrast to C_L in Fig. 9(a), the reduction rate of C_D with respect to h/C augments with increasing α in the range of $0^o \le \alpha \le 10^o$ as shown in Fig. 10(a).

Fig. 10(b) shows that, for $\alpha = 12°$, the maximum C_D occurs at the lowest h/C of 0.1, then decreases gradually as h/C increases up to 0.5, whereas, for $h/C > 0.5$, the value of C_D keeps almost constant. In the range of $14^o \le \alpha \le 30^o$, the variation of C_D with respect to h/C keeps almost the same pattern as that of the minimum C_D corresponding to the lowest h/C of 0.1. In the region $0.10 \le h/C \le 0.25$, C_D increases gradually, but it doesn't change too much even with increasing h/C in the range of $0.25 < h/C \le 1.25$. For constant h/C, C_D shows augmentation behavior as α increases.

In order to investigate the aerodynamic performance of the airfoil, the lift–to–drag ratio $f = C_L/C_D$ as function of the ground clearance for different angles of attack is depicted in Fig. 11. The behavior of f corresponding to the considered ground clearances and the angles of attack may be estimated from C_L and C_D that shown in Figs. 9 and 10, respectively. A comparison of the lift–to–drag ratio indicates that the best aerodynamic performance of the *GEV*, about 97, is obtained at $\alpha = 4^\circ$ and $h/C = 0.1$. Excluding its value at the lowest h/C, the smallest and highest $f's$ occur at $\alpha = 0°,and 6°$ respectively, both corresponds to the upper limit of h/C.

In the case of $\alpha = 12°$, the dramatic increment of f occurs beneath $h/C = 0.25,and 0.50$ as shown in Fig. 11(a). This jump of f for $\alpha = 12°$ is originated from the large reduction of C_D as already shown in Fig. 10(b). At a constant h/C in the range $\alpha \ge 14^\circ$, the *GEV* efficiency decreases as α increases.

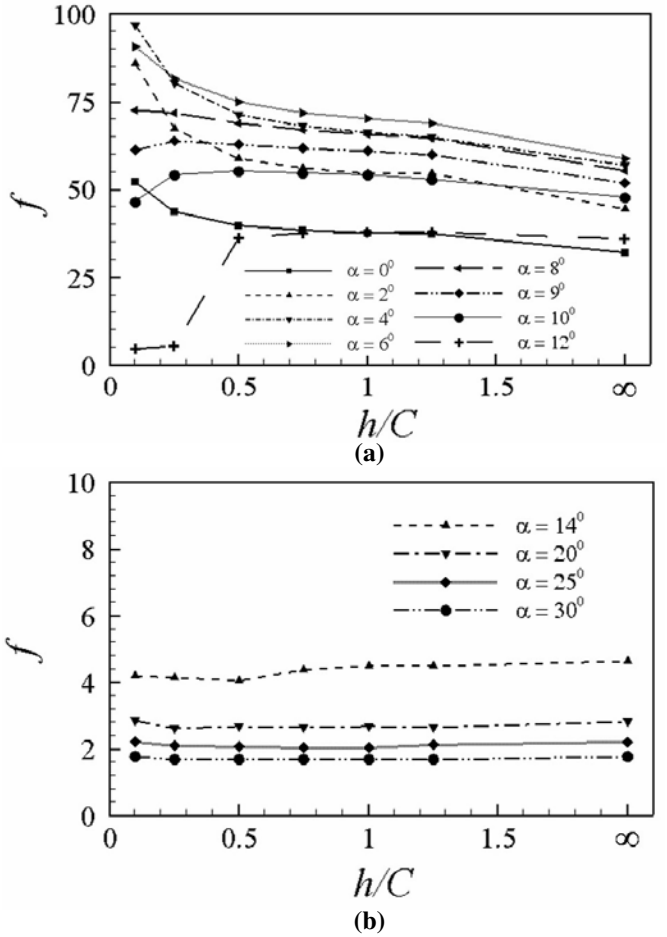

Fig. 11. Efficiency of the *GEV* as a function of the ground clearance for different angles of attack over the ranges of (a) $0^\circ \le \alpha \le 12^\circ$, and (b) $14^\circ \le \alpha \le 30^\circ$

EFFECT OF REYNOLDS NUMBER

Evaluating the aerodynamic characteristics of the *2-D WIG* of *NACA 4406* at $R_e = 2 \times 10^6$ in the wide ranges of the ground clearances $0.1 \le h/C \le 1.25$ and the angles of attack $0^o \le \alpha \le 30^o$ indicate that the best aerodynamic performance

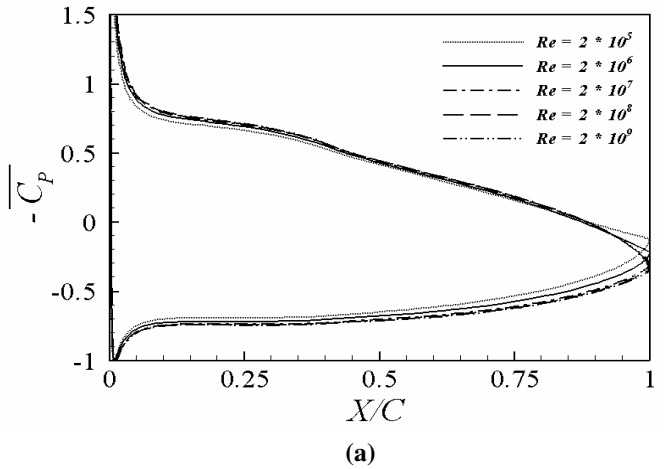

Fig. 12. Distribution of the mean pressure coefficient over the surface of the wing for different *Reynolds* numbers ranges as $2 \times 10^5 \le R_e \le 2 \times 10^9$ at $\alpha = 4^\circ$ and $h/C = 0.1$

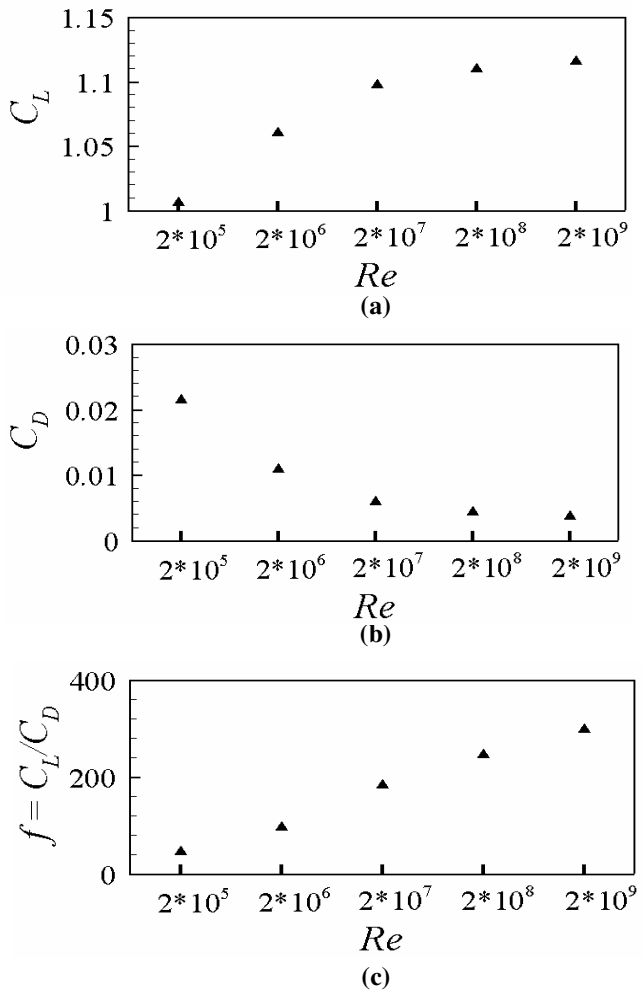

Fig. 13. (a) Lift coefficient, (b) drag coefficient and (c) lift-to-drag ratio as function of *Reynolds* number

with the highest value of the lift–to–drag ratio is obtained at $\alpha = 4^\circ$ and $h/C = 0.1$. Therefore, under such conditions of $\alpha = 4^\circ$ and $h/C = 0.1$, the effect of the *Reynolds* number on the distribution of the aerodynamic characteristics such as $\overline{C_P}$, C_L, C_D and f of the *2-D WIG* of *NACA 4406* is investigated in the range $2\times10^5 \le R_e \le 2\times10^9$.

Fig. 12 shows the variation of the mean pressure coefficient $\overline{C_P}$ on the wing surface at $\alpha = 4^\circ$ and $h/C = 0.1$ for different *Reynolds* numbers ranges as $2\times10^5 \le R_e \le 2\times10^9$. Regardless the magnitude of R_e, the distribution of $\overline{C_P}$ over the wing surface is analogous to that of $R_e = 2\times10^6$ as already discussed in Fig. 7(b). Consequently, over the whole range of the chord length, the pressure on the lower surface is higher than the corresponding pressure on the upper surface, which means the value of $-\overline{C_P}$ on the upper surface is larger than that on the lower surface as shown in Fig. 12. In other words, as R_e increases, the pressure on the upper surface decreases, whereas that on the lower surface increases, with the decrement and increment occurs at the same order of magnitude. This dependency of the pressure distribution on R_e is more distinguished by moving toward the trailing edge.

Fig. 13 shows the drag and lift coefficients together with the lift–to–drag ratio as functions of the *Reynolds* number R_e. As shown in Fig. 13(a), for $R_e < 2\times10^8$, C_L augments rapidly as R_e increases and eventually for $R_e \ge 2\times10^8$ C_L varies slowly. In contrast to C_L, C_D diminishes rapidly as R_e increases in the region $R_e < 2\times10^8$, and for $R_e \ge 2\times10^8$, it converges for any further increment in R_e as shown in Fig. 13(b). For the whole range of the *Reynolds* number $2\times10^5 \le R_e \le 2\times10^9$, as R_e increases, the lift–to–drag ratio increases almost linearly as shown in Fig. 13(c). The increment of f is governed by the linear relationship $f = \beta \times R_e$, where β is its slope and takes the approximate value of about 66.

CONCLUSIONS

The present study considers the numerical investigation of the *2-D WIG* problem, assuming that the flow is steady incompressible and viscous in order to simplify the physical problem. The commercial *CFD* package, *FLUENT 6.2*, is employed for all numerical calculations. The flow characteristics of the cambered airfoil *NACA 4406* have been numerically studied at various ground clearances ranges as $0.10 \le h/C \le 1.25$ for a wide range of angles of attack $0^o \le \alpha \le 30^o$ at $R_e = 2\times10^6$. Unequivocally, brief investigations of the principal conclusions that may be aggregated from the present research are furnished as follow:

a. In the range $0^\circ \le \alpha \le 10^\circ$, the mean flow shows almost the same pattern without the flow separation. However, as the angle of attack increases, the stagnation point slightly moves from the leading edge down toward the lower surface. At $\alpha = 12^o$ and $h/C = 0.1$, a primary vortex appears over the upper surface of the wing and it finally disappear as h/C increases further. For $\alpha \ge 14^o$ and $h/C = 0.1$, a secondary vortex appears between the primary one and the ground. As h/C increases, the secondary vortex disappears associated with diminishing the primary one as the increased gap predominates the downwash flow from the upper surface.

b. In general, the higher pressure distributes over the lower surface of the wing through its chord length because the cambered surface has a high flow divergence, regardless the magnitude of the angle of attack. As α exceeds 10°, the pressure distribution over the wing surface depends mainly on the vortex formed over the upper surface of the wing. Consequently, the deflection points of the pressure distribution over the upper surface appear near the vortex center and the reattachment point.

c. The air that is trapped between the wing and the runway forms an air cushion. The air cushion is created by higher pressure that builds up under the wing when the ground is approached. These are sometimes referred to as ram effect or ram pressure. When the ground distance becomes very small the air can even stagnate under the wing, giving the highest possible pressure; pressure coefficient of unity.

d. At $h/C = 0.1$, C_L has a maximum value in the range $0^o \le \alpha \le 12^o$ and a minimum value in the range $\alpha \ge 14^o$. For the range $0^o \le \alpha \le 6^o$, C_D slightly increases as h/C increases, with a maximum value appears in the range, $8^o \le \alpha \le 12^o$, and a minimum value appears in the range $14^o \le \alpha \le 30^o$, both occur at the minimum ground clearance $h/C = 0.1$. For the considered range of the angles of attack $0^o \le \alpha \le 30^o$, the variation of C_L and C_D may be neglected over a certain distance from the ground.

e. For the employed cambered airfoil and within the limits of the *IGE* and *OGE*, as the *GEV* efficiency $f = C_L/C_D$ increases with decreasing the ground clearance h/C, the craft becomes more efficient in ground effect, which means that those angles of attack α*'s* violating this condition should be avoided during landing the *WIG* vehicle. On the contrary side, those angles of attack which satisfy direct relationships between *GEV* efficiency and ground clearance h/C should be considered during taking off the *WIG* vehicle to avoid stall speed condition and consequently the highly probable crash of the *WIG* vehicle.

f. The higher the lift-to-drag ratio $f = C_L/C_D$, the higher the efficiency of the *WIG* vehicle and the lower its fuel consumption for a given weight. In the present study, the lift-to-drag ratio has a maximum value of 97 at $\alpha = 4^\circ$ and $h/C = 0.1$, which means for a vehicle in steady level, non-accelerating flight "stationary motion" flying at an angle of attack $\alpha = 4^\circ$ at a height $h/C = 0.1$, the amount of weight that may be carried with a certain amount of thrust is directly proportional to such thrust.

g. Studying the effect of the *Reynolds* number on the aerodynamic characteristics of *NACA 4406* for $\alpha = 4^o$ and $h/C = 0.1$ shows that C_L and C_D increases and decreases, respectively, as R_e increases in the range $2\times10^5 \le R_e \le 2\times10^9$. The dependency of C_L and C_D on the *Reynolds* number is significant throughout the region of the high *Reynolds* number. The *WIG* vehicle efficiency increases linearly as the *Reynolds* number increases. Although the present study does not consider a wider range of the ground clearances and the angles of attack, it clarifies the aerodynamic characteristics of the *WIG* effect at high *Reynolds* numbers.

This paper investigates aerodynamic characteristics of a wing in ground effect as a *2-D* flow problem, i.e. *chord dominated* wing in ground effect model in which the $height/chord$ represents the main parameter. However, a more realistic *3-D* model, i.e., *span dominated* wing in ground effect model in which the $height/span$ represents the main parameter should be investigated. Also, the influence of such realistic model on the induced drag and lift forces, and consequently the *vehicle efficiency* will be considered in the nearest future. Moreover, the effect of using an airfoil, from another family, on the aerodynamic characteristics of a wing in surface effect *WISE*, i.e., a wing in the vicinity of the free surface of *regular* and *irregular* wave systems will be considered.

NOMENCLATURE

C	Chord length of the wing, "*m*"
C_D	Drag coefficient $\left(C_D = D/0.5\rho U_\infty^2\right)$, "---"
C_L	Lift coefficient $\left(C_L = L/0.5\rho U_\infty^2\right)$, "---"
C_P	Pressure coefficient $\left(C_P = \left(P - P_{ref}\right)/0.5\rho U_\infty^2\right)$, "---"
D	Drag force, "*N*"
f	Lift–to–drag ratio, $\left(f = L/D = C_L/C_D\right)$, "---"
h	Vertical Distance from the trailing edge of the wing to the ground, "*m*"
L	Lift force, "*N*"
x	Dimension x axis coordinate, "*m*"
X	Transverse distance from the leading edge of the wing, "*m*"
y	Dimension y axis coordinate, "*m*"
Y	Vertical distance from the leading edge of the wing, "*m*"
R_e	*Reynolds* number $R_e = U_\infty C/\upsilon$, "---"
U_∞	Free-stream velocity, "*m/sec*"
α	Angle of attack, "*deg*"
β	Slop of the *GEV* efficiency with respect to the *Reynolds* number, "*rad*"
ρ	Density, "kg/m^3"
ν	Kinematic viscosity, "m^2/sec"

ACKNOWLEDGEMENTS

This research work was supported by Advanced Ship Engineering Research Center (ASERC) of Pusan National University through Korea Science and Engineering Foundation.

REFERENCES

[1] A. Nuhait, and D. Mook, "Numerical Simulation of Wings in Steady and Unsteady Ground Effects", *J. Aircraft*, 26, 1989, 1081-1089.

[2] N. Muzitani, and K. Suzuki, "Numerical Analysis of 3-D WIG Advancing over Still Water Surface", *J. the Society of Naval Architects of Japan*, 174, 1993, 35-46.

[3] C. Hsiun, and C. Chen, "Numerical Investigation of the Thickness and Camber Effects on Aerodynamic Characteristics for two-dimensional Airfoils with Ground Effect in Viscous Flow", *Trans. Japan Soc. Aero. Space Sci*, 38, 1995, 77-90.

[4] C. Hsiun, and C. Chen, "Aerodynamic Characteristics of a two-dimensional Airfoil with Ground Effect", *J. Aircraft*, 33, 1996, 386-392.

[5] H. Chun, and I. Park, "Analysis of Steady and Unsteady Performance for 3–D Air Wings in the Vicinity of the Free Surface", *Proc. a Workshop on Twenty–First Century Flying Ships, Sydney, Australia*, 1997, 23-46.

[6] C. Han, L. Cho, and J. Cho, "Wake Shapes Behind Wings in Close Formation Flight Near the Ground", *J. Mechanical Science and Technology*, 19:2, 2005, 674-681.

[7] Y. Moon, H. Oh, and J. Seo, "Aerodynamic Investigation of three-dimensional Wings in Ground Effect for Aero-

levitation Electric Vehicle", *Aerospace Science and Technology*, 9, 2005, 485-494.

[8] P. Fink, and L. Lastinger, "Aerodynamics Characteristics of Low-Aspect-Ratio Wings in Close Proximity to the Ground", *NASA TN D-926*, 1996.

[9] A. Carter, "Effect of Ground Proximity on the Aerodynamic Characteristics of Aspect Ratio: 1 Airfoils with and without Endplates", *NASA TN D-970*, 1961.

[10] H. Chun, "Experimental Studies on Wing-in-Ground Effect for three Different Wing Section Configurations", *Report NAOE-R-9604*, Dept. of NAOE, Pusan National University, Korea, 1996.

[11] H. Chun, K. Chung, and J. Chang, "Experimental Investigations on Wing in Ground Effect", *Proc. 3rd Korea-Japan Joint Workshop on Ship and Marine Hydrodynamics*, Daejon, Korea, 1996, 358-369.

[12] S. Kim, S. Suh, D. Lee, and K. Kim, "Wind Tunnel Test Study on the Wings of WIG Ship", *J. the Society of Naval Architects of Korea*, 34, 1997, 60-67.

[13] N. Ahmed, and J. Goonaratne, "Lift Augmentation of a Low-aspect-ratio Thick Wing in Ground Effect", *J. Aircraft*, 39, 2002, 381-384.

[14] J. Zerihan, and X. Zhang, "Aerodynamics of a Single Element Wing in Ground Effect, *J. Aircraft*, 37:6, 2000, 1058-1064.

[15] X. Zhang, J. Zerihan, A. Ruhrmann, and M. Deviese, "Tip Vortices Generated by a Wing in Ground Effect", *Proc. the 11th Int. Symp. on Applications of Laser Techniques to Fluid Mechanics*, Portugal, 2002.

[16] M. Ahmed, and S. Sharma, "An Investigation on the Aerodynamics of a Symmetrical Airfoil in Ground Effect", *Experimental Thermal and Fluid Science*, 29:6, 2005, 633-647.

[17] M. Shin, S. Yang, Y. Joo, S. Kim, Y. Bae, J. Kim, and H. Chun, "Wind Tunnel Test Results for Eight and Twenty Passenger Class WIG Effect Ships", *Proc. Int. Conf. on FAST Sea Transportation*, Sydney, Australia, 1997, 565-570.

[18] H. Chun, J. Chang, K. Paik, and S. Chang, "Preliminary Design of a 20 Passenger PARWIG Craft and Construction of a 1/10 Scale Radio Controlled Model", *Proc. Int. Conf. on FAST Sea Transportation*, Sydney, Australia, 1997, 513-520.

[19] C. Kong, H. Park, J. Yoon, and K. Kang, "Conceptual Design on Carbon-Epoxy Wing of a Small Scale WIG Vehicle", *Key Engineering Materials*, 334, 2007, 353-356.

[20] H. Chun and C. Chang, "Longitudinal Stability and Dynamic Motions of a Small Passenger WIG Craft", *Ocean Engineering*, 29, 2002, 1145-11.

[21] T. Shih, W. Liou, A. Shabbir, Z. Yang, and J. Zhu, "A New $k-\varepsilon$ Eddy- Viscosity Model for High Reynolds Number Turbulent Flows - Model Development and Validation", *Computers Fluids*, 24:3, 1995, 227-238.

[22] W. Reynolds, "Fundamentals of turbulence for turbulence modeling and simulation", *Lecture Notes for Von Karman*, Institute Agard, Report No. 755, 1987.

[23] S. Kim, D. Choudhury, and B. Patel, "Computations of Complex Turbulent Flows Using the Commercial Code FLUENT", *Proc. ICASE/LaRC/AFOSR Symp. on Modeling Complex Turbulent Flows*, Hampton, Virginia, 1997.